4b

GSI-95-01
PREPRINT
JANUAR 1995

LONGITUDINAL AND TRANSVERSE MOMENTUM DISTRIBUTIONS of ^{9}Li FRAGMENTS FROM BREAK-UP of ^{11}Li

F. HUMBERT, T. NILSSON, W. SCHWAB, M. ZINSER, Th. BLAICH, M.J.G. BORGE, L.V. CHULKOV, Th.W. ELZE, H. EMLING, B. FRANZKE, H. FREIESLEBEN, H. GEISSEL, K. GRIMM, D. GUILLEMAUD-MUELLER, P.G. HANSEN, R. HOLZMANN, H. IRNICH, L. JOHANNSEN, B. JONSON, J.G. KELLER, O. KLEPPER, H. KLINGLER, J.V. KRATZ, R. KULESSA, D. LAMBRECHT, Y. LEIFELS, A. MAGEL, M. MOHAR, A.C. MUELLER, G. MÜNZENBERG, P. MOELLER, F. NICKEL, G. NYMAN, A. RICHTER, K. RIISAGER, C. SCHEIDENBERGER, G. SCHRIEDER, B.M. SHERRILL, H. SIMON, K. STELZER, J. STROTH, O. TENGBLAD, W. TRAUTMANN, E. WAJDA, E. ZUDE

(Submitted to Phys. Lett. B)

Gesellschaft für Schwerionenforschung mbH
Postfach 11 05 52 · D-64220 Darmstadt · Germany

Longitudinal and transverse momentum distributions of ^{9}Li fragments from break-up of ^{11}Li

F. Humbert[1], T. Nilsson[2], W. Schwab[3], M. Zinser[3], Th. Blaich[4], M.J.G. Borge[5], L.V. Chulkov[6], Th.W. Elze[7], H. Emling[3], B. Franzke[3], H. Freiesleben[8], H. Geissel[3], K. Grimm[7], D. Guillemaud-Mueller[9], P.G. Hansen[10], R. Holzmann[3], H. Irnich[3], L. Johannsen[10], B. Jonson[2], J.G. Keller[8], O. Klepper[3], H. Klingler[7], J.V. Kratz[4], R. Kulessa[11], D. Lambrecht[4], Y. Leifels[8], A. Magel[3], M. Mohar[3], A.C. Mueller[9], G. Münzenberg[3], P. Møller[10], F. Nickel[3], G. Nyman[2], A. Richter[1], K. Riisager[10], C. Scheidenberger[3], G. Schrieder[1], B. M. Sherrill[12], H. Simon[1], K. Stelzer[7], J. Stroth[3], O. Tengblad[13], W. Trautmann[3], E. Wajda[11] and E. Zude[3]

December 13, 1994

1. Institut für Kernphysik, Technische Hochschule, D-64289 Darmstadt, Germany
2. Fysiska Institutionen, Chalmers Tekniska Högskola, S-41296 Göteborg, Sweden
3. Gesellschaft für Schwerionenforschung, D-64291 Darmstadt, Germany
4. Institut für Kernchemie, Johannes-Gutenberg-Universität, D-55099 Mainz, Germany
5. Insto. Estructura de la Materia, CSIC, E-28006 Madrid, Spain
6. Russian Scientific Center "Kurchatov Institute", Inst. Gen. and Nucl. Phys., Moscow 123182, Russia
7. Institut für Kernphysik, Johann-Wolfgang-Goethe-Universität, D-60486 Frankfurt, Germany
8. Institut für Experimentalphysik, Ruhr-Universität Bochum, D-44780 Bochum, Germany
9. Institut de Physique Nucléaire, IN2P3-CNRS, F-91406 Orsay Cedex, France
10. Institut for Fysik og Astronomi, Aarhus Universitet, DK-8000 Aarhus C, Denmark
11. Institute of Physics, Jagellonian University, PL-30-059, Poland
12. Michigan State University, East Lansing, MI 48824-1321, USA
13. PPE Division, CERN, CH-1211 Geneva 23, Switzerland

Abstract

Transverse and longitudinal momentum distributions of ^{9}Li fragments from ^{11}Li break-up reactions in C, Al and Pb targets have been measured at 280 MeV/u. The two-neutron removal cross-section was measured to be $\sigma_{-2n} = 0.26\pm0.02$ b for the carbon target, $\sigma_{-2n} = 0.47\pm0.08$ b for the aluminum target and $\sigma_{-2n} = 1.9\pm0.4$ b for the lead target. No significant difference is observed between the narrow widths (FWHM ≈ 47 MeV/c) of the transverse and longitudinal momentum distributions of the ^{9}Li fragments. The physical implications of this are discussed.

1 Introduction

Nuclear halos occur for nuclei very close to the drip line where the binding energy of the last nucleon, or pair of nucleons, is very low. Several nuclei showing halo phenomena are known and the by far most extensively studied case is ^{11}Li, which can be described as a Borromean three-body system [1] with two planetary neutrons orbiting the ^{9}Li core. The existing experimental results include matter radius, magnetic dipole and electric quadrupole moments, beta-decay properties, momentum distributions of neutrons and charged fragments after dissociation reactions and E1 excitation functions (see, for example, the recent reviews [2, 3, 4]). There is also a large theoretical literature available; special interest is attached to the three-body models [1], which, notwithstanding their basic simplicity, are expected to account for properties that are specific to a two-neutron halo.

Here we present the first results from new experiments combining for the first time the large high-energy facilities at GSI, the fragment separator (FRS), the dipole magnet (ALADIN) and the neutron detector (LAND). The aim of the present work was to study the momentum distributions of the ^{9}Li fragments after dissociation of ^{11}Li in collisions with light and heavy targets in both transverse and longitudinal directions at the same beam energy. The large acceptance of the spectrometers, both in longitudinal and transverse directions, give an undistorted picture of the fragment momentum distribution. Finally, the measurements at the same energy in both transverse and longitudinal directions for Pb targets indicate that core break-up limits the dissociation into core and valence neutrons to impact parameters much larger than grazing incidence.

2 Experimental Technique

The secondary beams were produced by fragmentation of a 340 MeV/u ^{18}O beam from SIS in an 8 g/cm^2 Be target. The production efficiency of ^{11}Li was measured to be $2.7\cdot10^{-7}$.

With a primary beam intensity of up to $2\cdot10^{10}$ ions/s, a secondary beam intensity of $5\cdot10^{3}$ ^{11}Li/s was achieved.

For the longitudinal momentum measurement, the fragment separator FRS [5] was used as an energy loss spectrometer. An ion-optical scheme of the FRS in the energy-loss mode is shown in Fig. 1 with envelopes in the direction of dispersion. With this technique, in first-order ion-optical imaging, the momentum spread caused by the ^{11}Li production process does not contribute to the measured width. At the central focal plane of the FRS the ^{11}Li beam with an energy of 280 MeV/u impinged on a secondary target of Al or Pb. In the following two ion-optical dipole stages of the FRS, the longitudinal momentum distribution of the emerging ^{9}Li fragments was determined from position spectra obtained at the final focal plane with multiwire chambers. The full longitudinal momentum distribution was obtained with *one* $B\rho$ setting. The spectra were transformed into momentum spectra (in the projectile frame) using the measured magnetic rigidity and the corresponding dispersion relation. Particle identification as well as absolute momentum determination was performed by additional time-of-flight measurements using scintillators and by measuring the energy deposition in an ionization chamber. The acceptance of FRS was ±105 MeV/c in the transverse momentum direction and ±60 MeV/c (in the projectile frame) for the longitudinal momentum, the latter being determined by the rigidity acceptance.

The transverse momentum distribution was measured at the ALADIN and LAND facilities. The experimental set-up is shown in Fig. 2. The exotic beams from the FRS were separated by pure magnetic rigidity analysis ($B\rho$), i.e. without a degrader. There was consequently no charge separation and the secondary beam was a mixture of the three drip line nuclei ^{8}He, ^{11}Li and ^{14}Be with energies of 240, 280 and 304 MeV/u, respectively. A minor contribution of ^{6}He at the same magnetic rigidity was also present. Since a direct beam line from the FRS to the experimental area was not available, it was necessary to send the beam through the experimental storage ring (ESR). This gave a strongly reduced transmission mainly due to a cut in the momentum acceptance, but at the same time considerably decreased the momentum spread of the secondary beam. At the experimental area typical beam intensities of 55, 50 and 10 ions per second of ^{8}He, ^{11}Li and ^{14}Be were obtained. For background corrections an experiment with an empty target frame was performed with similar statistics. The full width half maximum (FWHM) of the beam spot at the target was 2 cm. The angle and position of the incident ions were determined by means of a multiwire proportional chamber (MWPC) and a multiwire drift chamber (MWDC-1), placed 9 m apart. The charge identification of the different particles in the secondary beam was done event by event by measuring their energy loss in a 500 μm thick, position-sensitive plastic detector. This detector also provided the reference time for the events. The selection of charged fragments originating from reactions with the incident ^{11}Li beam was further improved by recording the time of flight between the plastic detector and a plastic wall. The small difference in velocity between beam and fragment makes this method very reliable. The fragments emerging from the secondary target were deflected and separated according to their rigidity in a large-gap magnetic spectrometer, ALADIN [6], with a bending power of 2 Tm and detected by two MWDC's. The wire planes of these

MWDC's consist of alternating anode and cathode wires with a maximum drift distance of 5 mm. A position resolution of <2 mm was achieved by using a delay-line technique [7]. The charges of the fragments were determined by measuring the energy loss (ΔE) in the plastic wall.

3 Data treatment and results

In the longitudinal momentum measurement with the FRS the contributions to the position distribution from multiple angular scattering and energy-loss straggling as well as ion-optical image aberrations were taken into account by the corresponding transmission measurements of the ^{11}Li through the same secondary targets. The use of the secondary target with a constant thickness along the direction of dispersion deteriorated the achromatism of the FRS. This gives a weak dependence of the position at the final focal plane on the ^{11}Li momentum. A correction for this was performed which reduced the measured width by several percent. With a determination of the magnetic field to better than 10^{-4} and with a position resolution of the ray-tracing detectors of 2 mm the momentum width could be measured with a 5 % uncertainty. The effect of the finite transverse acceptance, see also the discussion, can be readily simulated [10] and amounts in the present case to a 4 % decrease of FWHM. The data have been corrected for this and we have, in order to give conservative error bars, included the correction term as a systematic error. Fig. 3 shows the longitudinal momentum distribution measured with the aluminum and lead targets. The intrinsic width was extracted by fitting the data with a Lorentzian folded with the instrumental resolution (see above) and compensating for the limited acceptance. The two-neutron removal cross-sections was here measured to be σ_{-2n}=0.47±0.08 for the aluminium target and σ_{-2n}=1.9±0.4 for the lead target. Table 1 gives the measured momentum width, the width of the non-reacting ^{11}Li beam and the deduced FWHM of the momentum distribution.

In the experiment at ALADIN-LAND the reaction channel was identified unambiguously from the ΔE-information and time of flight, provided by the position-sensitive plastic detector and the plastic wall, together with the MWDC-data. The $^{11}\text{Li} \rightarrow {}^{9}\text{Li}$+X-events were selected by imposing two-dimensional cuts on the x-position in MWDC-2 as a function of the difference in x-position between MWDC-2 and MWDC-3. The latter entity approximately corresponds to the bending angle in ALADIN. This method yields an excellent separation between ^{11}Li and ^{9}Li as seen in the lower inset of Fig. 2. The two-neutron removal cross-sections were obtained as σ_{-2n}=0.26±0.02 b and σ_{-2n}=1.9±0.7 b for the carbon and lead target, respectively. In addition to the ^{9}Li events we also observed a broad distribution of ^{8}Li fragments in coincidence with neutrons. This latter component contained about 25% of the observed ^{9}Li intensity for the Pb target.

The ^{9}Li transverse momentum distributions were extracted from the y-position in MWDC-

2 and are thus virtually undisturbed by the bending in the magnetic field. To correct for the spatial spread of the incident beam the y-position in MWDC-1 was subtracted from the position in MWDC-2. The distribution without target, which was used for background subtraction, is too narrow since no target angular straggling contributes. The straggling was deduced by comparing the non-reacting ^{11}Li distribution with and without target and this was then folded into the no-target distribution. Fig. 3 shows the transverse momentum distribution after background corrections for the lead target. The momentum spread of the beam, due to multiple scattering in the detectors, target, air etc., was extracted from the ^{11}Li distribution perpendicular to the bending plane and was used to deduce the momentum widths.

The best fit to the experimental data was here clearly obtained with a Lorentzian shape. A two Gaussian fit, as used in ref. [8] included too many free parameters and did not give a reasonable result. The FWHMs given in Table 1 represent distributions where integrations along the beam axis and a direction perpendicular to it were performed. It should be noted that a distribution on p_y is different from the more conventional distribution on radial momentum $p_\perp$.

4 Discussion

In this experiment results on the transverse as well as on the longitudinal momentum distributions were obtained at the same ^{11}Li beam energy after break-up in both a low Z and a high Z target. The general observation is that the widths are almost identical, 47 MeV/c, in all cases.

The parallel momentum widths of ^{9}Li fragments have earlier been measured at 66 MeV/u by Orr et al. [9] with the A1200 spectrometer at MSU. They observed a weak decrease in the width with increasing target charge and a similar trend between Al and Pb is marginally indicated by our data. The measured widths in the MSU experiment were smaller than what we found at 280 MeV/u by about 5 MeV/c. Without excluding a real dependence of the width on beam energy, we wish here to note that such a result also can be caused by a difference of the two instruments. The underlying mechanism can be illustrated with a schematic model. Let us assume that the momentum distribution after the reaction can be described as a three-dimensional Lorentzian

$$w(\mathbf{p})d\mathbf{p} = \frac{\Gamma}{2\pi^2}\frac{d\mathbf{p}}{(p_x^2 + p_y^2 + p_z^2 + \Gamma^2/4)^2}. \tag{1}$$

Experimentally a projection of this distribution is observed. If the z-projection is observed with an instrument having 100% acceptance in the transverse directions (which is close to being the case for the FRS) the result will correspond to an integration of eq. (1) in the x and y directions. The distribution function is then

$$w_2(p_z) = \frac{\Gamma}{2\pi(p_z^2 + \Gamma^2/4)} \tag{2}$$

so that the experimental FWHM directly gives Γ. The effect of a selection of small momentum components is illustrated in the limit of vanishing p_x and p_y where the distribution function becomes

$$w_2(p_z) \propto \frac{1}{(p_z^2 + \Gamma^2/4)^2}. \tag{3}$$

The FWHM of this distribution is $\Gamma\sqrt{2^{1/2} - 1} = 0.644\Gamma$. Limitations in acceptance would result in a FWHM between these extremes.

Turning now to the transverse momentum width we must here include the contribution from deflection of the ^{9}Li core in the Coulomb field of the target nucleus. We have estimated this contribution using simple models [11] of the Coulomb and nuclear dissociation probabilities. We find that this effect will give a large contribution only for nuclear dissociation in the Pb target, while in the other cases it will be less than the spread from the beam profile. Based on an extrapolation of the 0.26 b pure nuclear break-up for the carbon target following ref. [12] one would expect a nuclear contribution to the cross section of more than 0.5 b for the lead target. This would result in a broadening of the distribution of more than 10 MeV/c since the major nuclear contribution stems from the first 5-6 fm region outside grazing incidence, $b = R_c + R_T$ [13]. However, the data in Table 1 show the widths of the longitudinal and transverse momentum distributions for the Pb target are the same within the experimental uncertainty. It appears thus that for impact parameters below $b = R_c + R_T$ plus a few fm, the ^{9}Li core is also likely to break up. A depopulation of the ^{9}Li+2n reaction channel into for example ^{8}Li+3n would then occur and the broad ^{8}Li transverse momentum distribution ($\Gamma \approx 140$ MeV/c), which has a cross-section of about 0.5 b, is in support of such an interpretation. Our widths are slightly smaller than the ones obtained on D and C targets at 800 MeV/u [14, 8], but the interpretation agrees well with the recent results from RIKEN [15] on ^{11}Be+Pb→ ^{10}Be+n+X where dissociations of this type were observed only to take place at impact parameters larger than 12 fm. The large discrepancy between our result and the one given in ref. [14] for the Pb target (Γ=167±35 MeV/c) may be due to multiple scattering in the twenty times thicker target used in that experiment.

The Coulomb 2n-removal cross-section for the reaction ^{11}Li→^{9}Li+X has been calculated [16] for a Pb target. The ground state and continuum wave functions for ^{11}Li, used in the calculation, were obtained using the hyperspherical harmonics method (HH) in the framework of a three-body model as described in ref. [17]. The E1 strength function according to ref. [18] (version H) was used. The result is σ_{-2n}^{C}= 1.23 b which indicates that the observed total 2n-removal cross-section, σ_{-2n} = 1.8±0.4 b is of the same magnitude as the expected Coulomb part. This further supports the interpretation given above.

In summary, we have observed almost identical longitudinal and transverse momentum distributions of ^{9}Li fragments from break-up of ^{11}Li on light as well as heavy targets. This is somewhat surprising since one would expect the break-up mechanism to noticably influence at least the transverse distribution from heavy targets. We suggest that this could be caused by break-up of ^{9}Li for small impact parameters. The other distributions have been suggested [8, 9, 14] to reflect directly the momentum distribution in the halo ground state. Interpreted in this way our data imply a value of $\Gamma = 47$ MeV/c which, due to the large acceptance and the thin targets used, is the presently most accurate value obtained at high beam energy.

5 Acknowledgements

The authors are indebted to M. V. Zhukov for discussions and suggestions. We also thank I. J. Thompson for calculating the Coulomb cross-sections. This work was supported by the German Federal Minister for Research and Technology (BMFT) under Contracts 06 DA 641 I, 06 BO 103 and 06 MZ 106 and by GSI via Hochschulzusammenarbeitsvereinbarungen under Contracts DA RICK, BO FRE, F ELE, Mz KRD and partly supported by the Polish Committee of Scientific Research under Contract PB1158/P3/92/02 and CICYT under contract AEN92-0788-C02-02 (MJGB).

References

[1] M.V. Zhukov, B.V. Danilin, D.V. Fedorov, J.M. Bang, I.J. Thompson and J.S. Vaagen, Phys. Rep. 231 (1993) 151.

[2] P.G. Hansen, Nucl. Phys. A553 (1993) 89c.

[3] T. Kobayashi, Nucl. Phys. A553 (1993) 343c.

[4] B. Jonson, Nucl. Phys. A574 (1994) 151c

[5] H. Geissel, P. Ambruster, K. H. Behr, A. Brünle, K. Burkard, M. Chen, H. Fogler, B. Franczak, H. Keller, O. Klepper, B. Langenbeck, F. Nickel, E. Pfeng, M. Pfützner, E. Roeckl, K. Rykaczewski, I. Schall, D. Schardt, C. Scheidenberger, K.-H. Schmidt, A. Schröter, T. Schwab, K. Sümmerer, M. Weber, G. Münzenberg, T. Brohm, H.-G. Clerc, M. Fauerbach, J.-J. Gaimard, A. Grewe, E. Hanelt, B. Knödler, M. Steiner, B. Voss, J. Weckenmann, C. Ziegler, A. Magel, H. Wollnik, J.P. Dufor, Y. Fujita, D.J. Viera and B. Sherrill, Nucl. Instr. Meth. B70 (1992) 286.

[6] The ALADIN Collaboration, GSI Scientific Report, Darmstadt, (1989) 292.

[7] R.S. Henderson, O. Hausser, K. Hicks, C. Gunter, W. Faszer, R. Sawafta and N. Poppe, Nucl. Instr. Meth. A254 (1987) 61.

[8] I. Tanihata, T. Kobayashi, T. Suzuki, K. Yoshida, S. Shimoura, K. Sugimoto, K. Matsuta, T. Minamisono, W. Christie, D. Olson and H. Wieman, Phys. Lett. B287 (1992) 307.

[9] N. A. Orr, N. Anantaraman, Sam M. Austin, C. A. Bertulani, K. Hanold, J. H. Kelley, D. J. Morrissey, B. M. Sherrill, G. A. Souliotis, M. Thoennessen, J. S. Winfield and J. A. Winger, Phys. Rev. Lett. 69 (1992) 2050.

[10] K. Riisager, dr. scient thesis, Aarhus University (1994), unpublished

[11] R. Anne, R. Bimbot, S. Dogny, H. Emling, D. Guillemaud-Mueller, P. G. Hansen, P. Hornshøj, F. Humbert, B. Jonson, M. Keim, M. Lewitowicz, P. Møller, A. C. Mueller, R. Neugart, T. Nilsson, G. Nyman, F. Pougheon, K. Riisager, M. G. Saint-Laurent, G. Schrieder, O. Sorlin, O. Tengblad and K. Wilhelmsen Rolander, Nucl. Phys. A575 (1994) 125

[12] D. L. Olson, B. L. Berman, D. E. Greiner, H. H. Heckman, P. J. Lindstrom and H. J. Crawford, Phys. Rev. C28 (1983) 1602.

[13] Y. Ogawa, K. Yabana and Y. Suzuki, Nucl. Phys A543 (1992) 722.

[14] T. Kobayashi, O. Yamakawa, K. Omata, K. Sugimoto, T. Shimoda, N. Takahashi and I. Tanihata, Phys. Rev. Lett. 60 (1988) 2599.

[15] T. Nakamura, S. Shimoura, T. Kobayashi, T. Teranishi, K. Abe, N. Aoi, Y. Doki, M. Fujimaki, N. Inabe, N. Iwasa, K. Katori, T. Kubo, H. Okuno, T. Suzuki, I. Tanihata, Y. Watanabe, A. Yoshida and M. Ishihara, Phys. Lett. B331 (1994) 296

[16] I. J. Thompson, private communication 1994.

[17] M.V. Zhukov, B.V. Danilin, D.V. Federov, J.S. Vaagen, F.A. Gareev and J.M. Bang, Phys. Lett. B265 (1991) 19.

[18] B.V. Danilin, I.J. Thompson, M.V. Zhukov, J.S. Vaagen and J.M. Bang, Phys. Lett.B (1994) in press.

Table 1: Momentum widths of ^{9}Li fragments after break-up of ^{11}Li

Distribution	Target (Thickness, g/cm^2)	Exp. FWHM (MeV/c)	Beam FWHM (MeV/c)	Deduced FWHM^b (MeV/c)	χ^2_N ^{c}
p_y	C (1.293)	72	41	45±4	1.9
p_y	Pb (0.302)	73	42	49±4	0.8
$p_{\parallel}$ ^{a}	Al (5.4)	54	15	49±3	1.3
$p_{\parallel}$ ^{a}	Pb (8.0)	51	15	45±3	0.9

a) The values refer to a coordinate system moving with the projectile.
b) The distributions have been integrated over two momentum directions meaning that the FWHM corresponds directly to the Γ parameter defined in eq. (1).
c) Normalized χ^2

Figure Captions

Figure 1 Schematic view of the FRS in the energy-loss mode [5]. The upper part of the figure shows how, without a secondary target, the ^{11}Li beam with large momentum and angle spread is focussed achromatically onto a single spot in the final focal plane. In the lower part it is shown how a small momentum change in the target, resulting from the longitudinal momentum distribution of the break-up of the secondary beam particle, can be measured precisely by a position change in the last focal plane. Thus, although the spread of the secondary beam is large ($\Delta p/p > 1\%$) the longitudinal momentum can be determined with an accuracy of $\Delta p/p < 10^{-3}$. Measured position distributions at the focal plane are displayed for ^{11}Li and ^{9}Li in the secondary Pb target.

Figure 2 The experimental set-up in Cave B at the GSI. The incoming ^{11}Li beam position is defined by a MWPC when entering the cave and by MWDC-1 just in front of the secondary target. After the target the beam and the fragments from the reactions are analysed according to momenta and direction by the ALADIN spectrometer in conjunction with two drift chambers (MWDC-2,3). The inset in the upper left corner shows the position information in MWDC-2. The plastic wall, consisting of seven segments with 10 mm thickness, is used to obtain time-of-flight and charge information. The combined information from this configuration allows a clean identification of the charged fragments. The separation for Z=3 is shown in the lower inset. The neutrons from the reactions are detected according to position and time-of-flight in a large area neutron detector (LAND).

Figure 3 Measured longitudinal and transverse momentum distributions of ^{9}Li after dissociation of 280 MeV/u ^{11}Li. Note that the apparent difference in width of these distributions is due to different experimental broadenings (see Table 1). The FRS data have been fitted with a truncated Lorentzian to model the decreasing acceptance from 100% to 0% within 20 MeV/c.

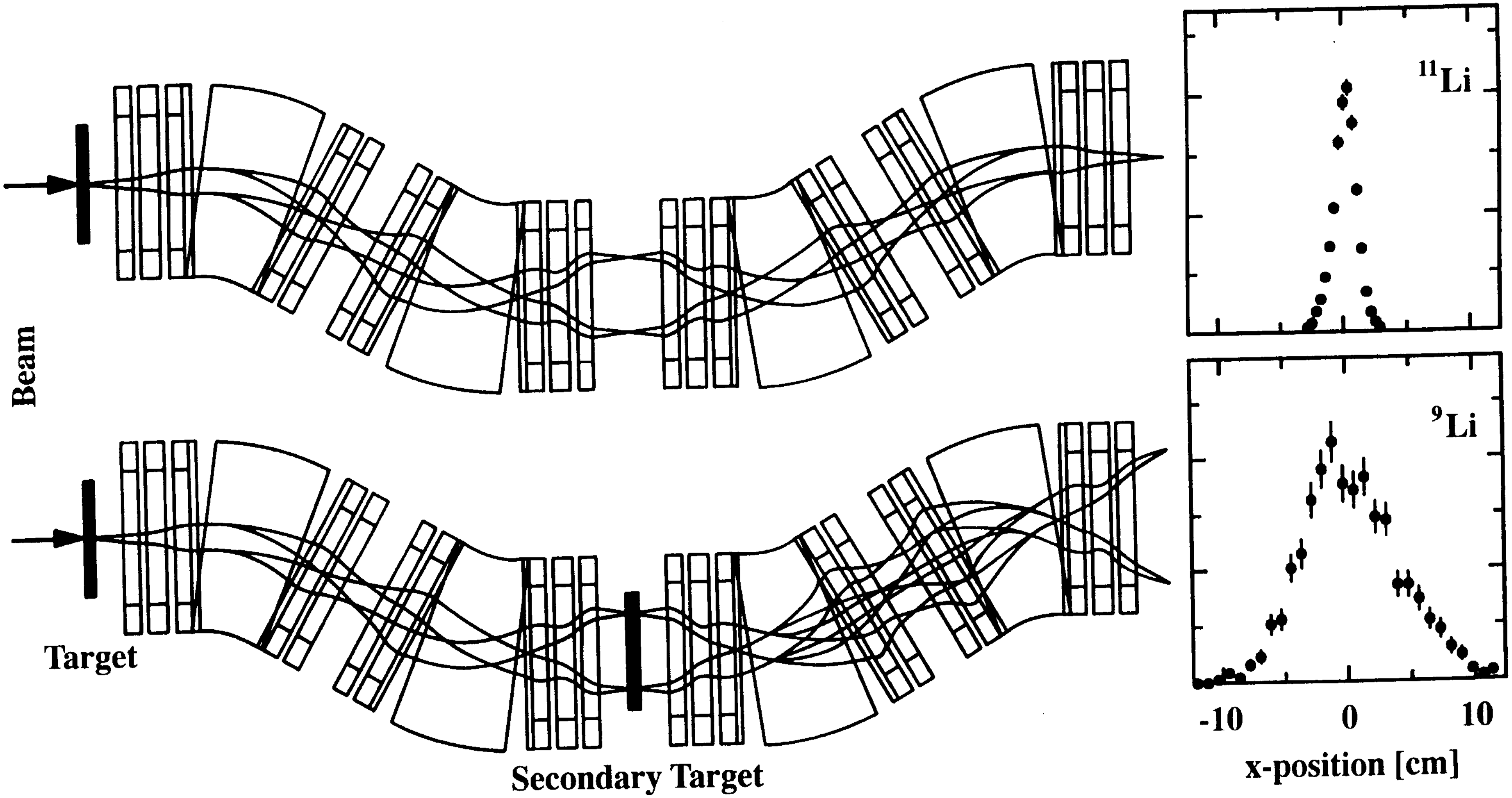
Beam
Target
Secondary Target
^{11}Li
^{9}Li
-10
0
10
x-position [cm]

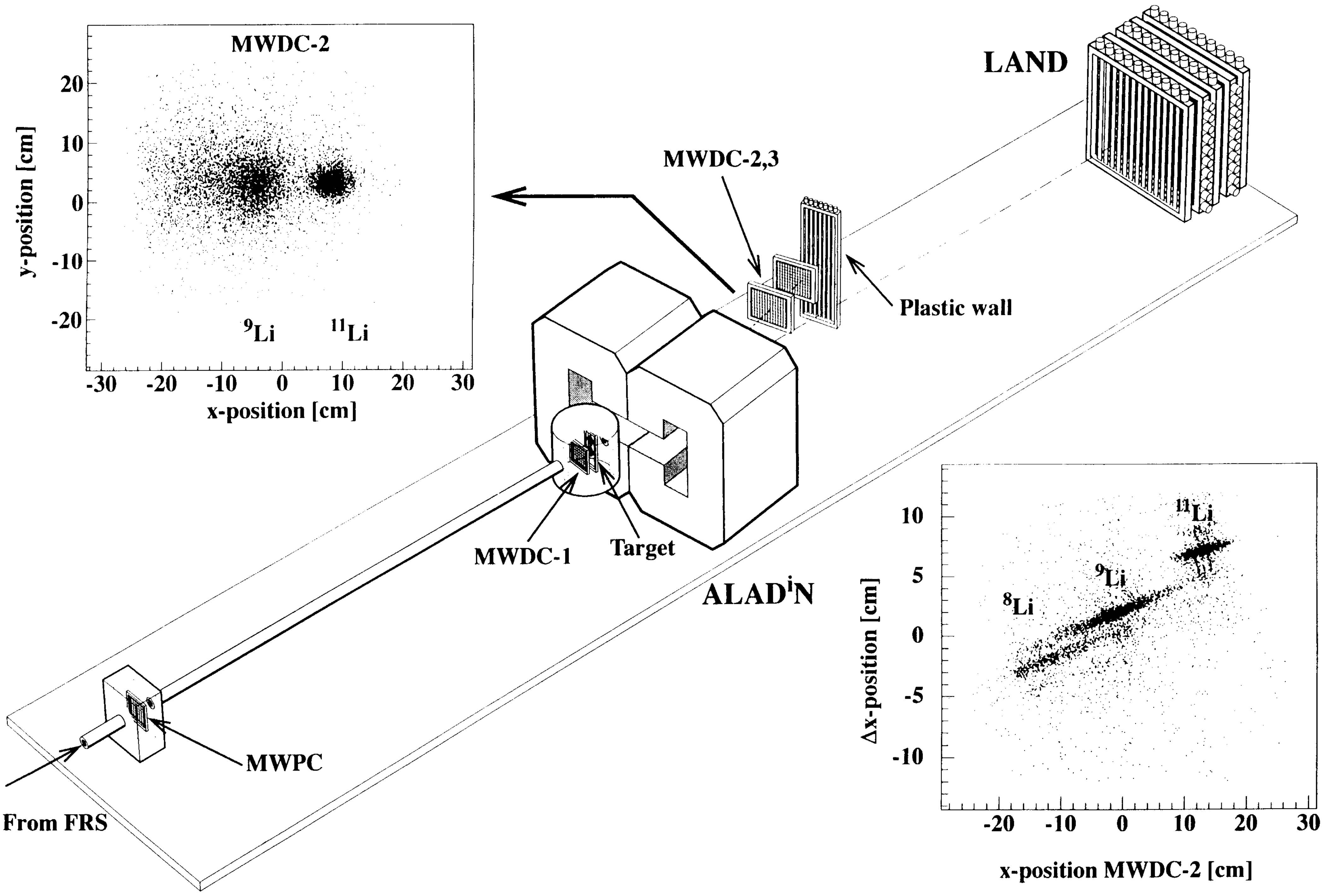
MWDC-2
20
10
0
-10
-20
y-position [cm]
^{9}Li
^{11}Li
-30
-20
-10
0
10
20
30
x-position [cm]
LAND
MWDC-2,3
Plastic wall
MWDC-1
Target
ALAD^{i}N
MWPC
From FRS
^{11}Li
^{9}Li
^{8}Li
10
5
0
-5
-10
Δx-position [cm]
-20
-10
0
10
20
30
x-position MWDC-2 [cm]

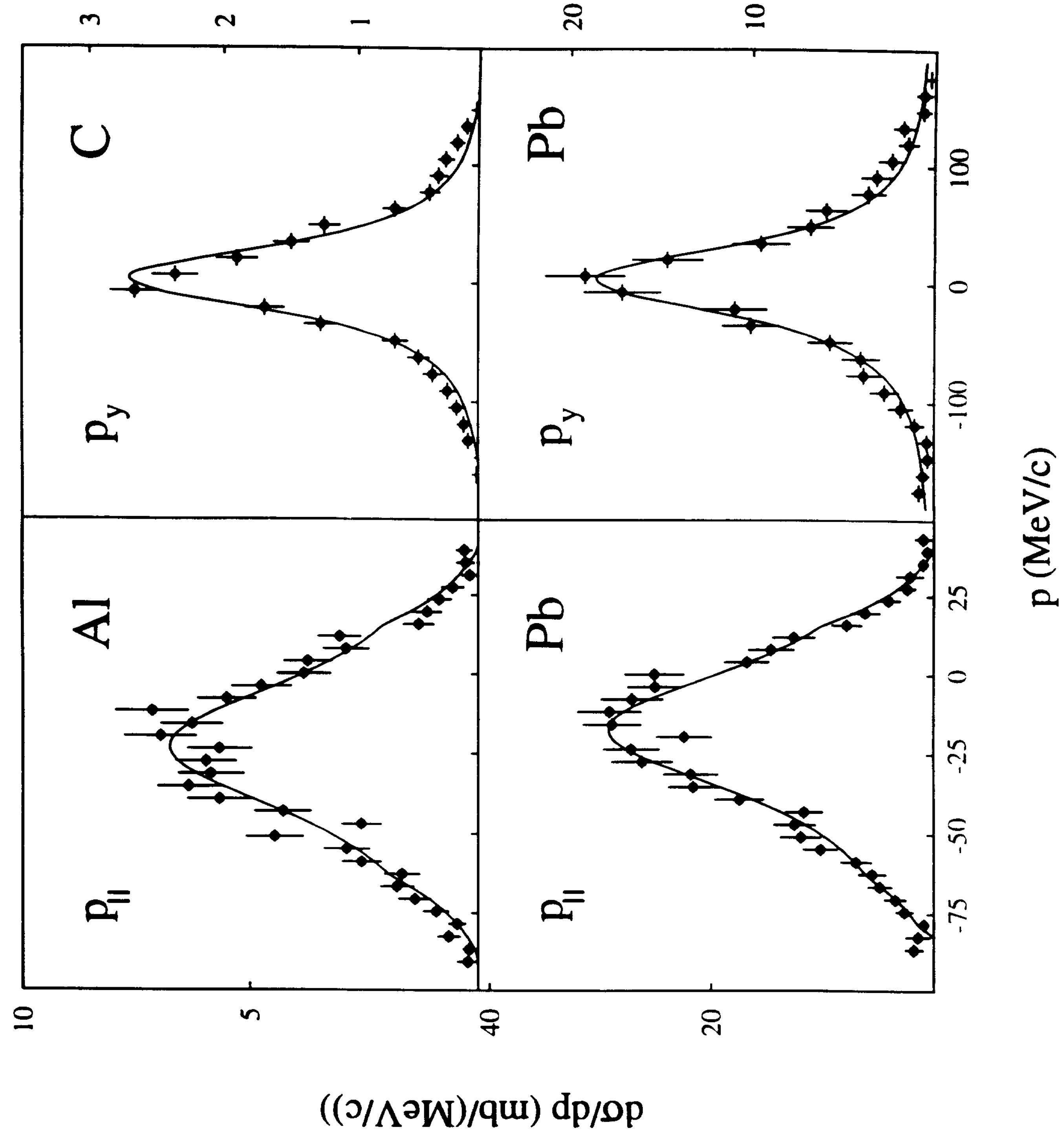
Al
C
Pb
Pb
$p_{||}$
p_y
$p_{||}$
p_y
dσ/dp (mb/(MeV/c))
p (MeV/c)
10
5
40
20
3
2
1
20
10
-75
-50
-25
0
25
-100
0
100